



# Dilatometric analysis of sintering lithium-titanium-zinc ferrite with ZrO<sub>2</sub> additive

Svetlana A. Nikolaeva<sup>1</sup> · Elena N. Lysenko<sup>1</sup> · Evgeniy V. Nikolaev<sup>1</sup> · Anatoliy P. Surzhikov<sup>1</sup>

Received: 13 July 2020 / Accepted: 16 November 2020 / Published online: 4 January 2021  
© Akadémiai Kiadó, Budapest, Hungary 2021

## Abstract

Sintering of multicomponent lithium ferrite of the chemical composition Li<sub>0.65</sub>Fe<sub>1.6</sub>Ti<sub>0.5</sub>Zn<sub>0.2</sub>Mn<sub>0.05</sub>O<sub>4</sub> with the addition of ZrO<sub>2</sub> was studied using dilatometric and kinetic analyses. The LiTiZn ferrite was synthesized by solid state reaction from Fe<sub>2</sub>O<sub>3</sub>, Li<sub>2</sub>CO<sub>3</sub>, TiO<sub>2</sub>, ZnO, and MnO<sub>2</sub> high-purity powders, and then doped with zirconia nanopowder (0.5, 1 and 2 mass%). The ZrO<sub>2</sub> was prepared by sol–gel technique. It was found that small concentration of ZrO<sub>2</sub> additives (up to 1 mass%) increase the bulk density of ferrite. An increase in the concentration of ZrO<sub>2</sub> additive to 2 mass% causes deterioration of ferrite compaction. Shrinkage curves were used to perform the kinetic analysis based on mathematical modeling to find the parameters of ferrite sintering. The kinetic analysis showed that the diffusion models are suitable for mathematical determination of the kinetic patterns of ferrite sintering. The estimated values of the kinetic parameters can be used to improve the technological process of sintering of multicomponent ferrite materials doped with zirconia.

**Keywords** Lithium-titanium-zinc ferrite · ZrO<sub>2</sub> additive · Sintering · Dilatometry · Kinetic analysis

## Introduction

Soft ferrites belong to the category of promising materials due to their widespread use [1]. The area of ferrite application depends on the type of its structure. For example, spinel lithium ferrites due to their good magnetic and electrical properties are widely used in microwave devices and other applications as magnetic fluids, high-density magnetic recording, gas sensors, etc. [2–8]. Lithium-substituted ferrites with Fe<sup>3+</sup> ions replaced by zinc or titanium ions are characterized by low dielectric losses and high temperature stability, which explains the demand for their use in microwave technology [9–13]. Specifically, multicomponent lithium ferrites with the Li<sub>0.5+0.5t–0.5x</sub>Fe<sub>2.5–1.5t–0.5x</sub>Ti<sub>t</sub>Zn<sub>x</sub>O<sub>4</sub>

chemical formula is widely used as discrete phase shifters, where density of the material is crucial for formation of electromagnetic properties [14, 15].

It is well known that the properties of ferrites can be improved by additives [16–18]. Thus, zirconia additives used to improve the properties and structural state of a wide class of powder materials are becoming increasingly popular [19–23]. The findings of the previous studies [24–28] show that this additive affects the ferrite structure. This enables the control of structurally sensitive properties, such as electrical conductivity, magnetic permeability, thermal conductivity, and the shape of the hysteresis loop.

In our previous studies [29, 30], we investigated the effect of the unstabilized ZrO<sub>2</sub> nanopowder additive produced by the plasma-chemical method on the structure and properties of solid-phase sintered lithium and lithium-substituted ferrites. It was shown that introduction of ZrO<sub>2</sub> additive in small concentration of up to 2 mass% increases the density of lithium-titanium-zinc ferrites thus improving ferrite parameters such as microhardness, electrical resistivity, and saturation magnetization. However, an increased concentration of the additive introduced to 3 mass% causes decrease in density and increase in porosity of sintered ferrites.

The aim of this study is to investigate the effect of small concentration of ZrO<sub>2</sub> additives prepared by sol–gel

✉ Elena N. Lysenko  
lysenkoen@tpu.ru

Svetlana A. Nikolaeva  
sal17@tpu.ru

Evgeniy V. Nikolaev  
nikolaev0712@tpu.ru

Anatoliy P. Surzhikov  
surzhikov@tpu.ru

<sup>1</sup> Tomsk Polytechnic University, Lenin Avenue 30, Tomsk, Russia 634050

technique on the solid-phase sintering process of multi-component lithium ferrite. It can be noted that the sol–gel method is a modern way of obtaining high-purity, homogeneous and crystalline nanoparticles at low processing temperatures [31–33]. In addition, ZrO<sub>2</sub> nanopowder is widely used in chemical technologies and in research [34].

In the present study, LiTiZn ferrite sintering processes were analyzed by the dilatometric method, that is high temperature compaction of samples accompanied by reduction of external dimensions (shrinkage) was studied. The results of the dilatometric studies were used to conduct the kinetic analysis in order to determine the kinetic parameters and a sintering model for further adjustment of the process parameters in manufacturing multicomponent ferrite materials.

## Experimental

Ferrite powder was synthesized in accordance with the Li<sub>0.65</sub>Fe<sub>1.6</sub>Ti<sub>0.5</sub>Zn<sub>0.2</sub>Mn<sub>0.05</sub>O<sub>4</sub> chemical formula using solid state reaction from Fe<sub>2</sub>O<sub>3</sub> (60.38 mass%), Li<sub>2</sub>CO<sub>3</sub> (11.35 mass%), TiO<sub>2</sub> (18.9 mass%), ZnO (7.7 mass%), and MnO (1.67 mass%) high-purity powders. Mixture of reagents was produced by weighing the required amount of pre-dried components and then was dry-mixed in an AGO-2S ball mill at 2220 rpm using 5-mm steel grinding balls. The milling time was 60 min. The synthesis of LiTiZn ferrite was performed in a resistance furnace at 900 °C for 240 min. As shown in [29], the crystal structure of LiTiZn ferrite synthesized in this way is a single phase spinel with the lattice parameter of 8.3600 Å. After synthesis, Bi<sub>2</sub>O<sub>3</sub> in the amount of 1 mass% was added to LiTiZn ferrite powder in order to decrease the sintering temperature and prevent the volatilization of lithium from ferrite during its sintering.

The prepared powder was divided into four equal parts. The ferrite powder from the first part was without ZrO<sub>2</sub> additives (sample N1). ZrO<sub>2</sub> nanopowder stabilized by 3 mol% Y<sub>2</sub>O<sub>3</sub> (Tosoh Corporation, Japan) was added to the other powder parts by gradual mixing in different percentages (0.5, 1 and 2 mass% in samples N2, N3, N4, respectively). To ensure a more accurate percentage of zirconia in ferrite, the powders were dried for 3 h at 200 °C in an oven before weighing to eliminate the possible moisture of the powders. Thorough mixing of ZrO<sub>2</sub> in the entire volume of the multicomponent ferrite powder was carried out in a planetary ball mill at 300 rpm for 30 min.

The resulting powder of 0.5 g in mass was compacted in the form of pellets with a diameter of 9 mm and an average thickness of about 2.6 mm. Compaction was performed using a hydraulic press PGR-10 with a constant load of 1.3 tons for 3 min.

Sample shrinkage during sintering was studied by the dilatometric method using a highly sensitive DIL 402C

dilatometer. The measurement results were corrected with regard to the preliminary calibration on a standard corundum sample in order to determine the contribution of linear thermal expansion of the pusher and the sample holder to the results. The N1, N2, N3, and N4 samples were heated in air at a constant rate of 10 °C min<sup>-1</sup> to sintering temperature of 1010 °C with subsequent isothermal exposure for 120 min. As shown in [35], when using a sintering temperature of 1010 °C, LiTiZn ferrites are characterized by improved structural and magnetic properties.

The bulk density of the samples was calculated before and after sintering by hydrostatic weighing using distilled water (Table 1). Measurement errors for bulk densities are ca. 0.2–0.3%.

The kinetic analysis of LiTiZn ferrite sintering was carried out using the mathematical modeling of dilatometric shrinkage curves measured at several heating rates of 2, 5, and 10 °C min<sup>-1</sup>. The goal of the kinetic analysis was to provide mathematical description of solid-phase reactions and to find a kinetic model with optimal reaction parameters, which can help to quantitatively describe the kinetics of the process [36]. In this study, modeling was performed using Netzsch Thermokinetics 3.1 software.

The kinetic model of the reaction and parameters characterizing this sintering process are used to optimize the technological conditions for ferrite production [37–39]. The basic equation for the kinetic analysis is represented by the following expression:

$$d\alpha/dt = k \cdot f(\alpha) \quad (1)$$

where  $\alpha$  is a conversion degree,  $f(\alpha)$  is the temperature-independent function of the conversion ratio,  $k$  is Arrhenius equation:

$$k = A \cdot \exp\left(-\frac{E_a}{RT}\right) \quad (2)$$

where  $A$  is a pre-exponential factor,  $E_a$  is activation energy,  $T$  is absolute temperature, and  $R$  is the gas constant (8.314 J K<sup>-1</sup> mol<sup>-1</sup>).

The final expression for the kinetic analysis is as follows:

**Table 1** The bulk density of the samples

Sample	ZrO <sub>2</sub> content/ mass%	Density before sintering/g cm <sup>-3</sup>	Density after sintering/g cm <sup>-3</sup>
N1	0	2.86	4.27
N2	0.5	2.87	4.30
N3	1	2.85	4.31
N4	2	2.88	3.38

$$d\alpha/dt = A \cdot \exp\left(-\frac{E_a}{RT}\right) \cdot f(\alpha) \tag{3}$$

In dilatometric measurements, the conversion degree is calculated as follows:

$$\alpha = \frac{L_0 - L_t}{L_0 - L_f} \tag{4,}$$

where  $L_0$  is the initial thickness of the sample;  $L_t$  is the sample thickness at time  $t$ ;  $L_f$  is the final thickness of the sample.

The initial stage of the kinetic analysis implies estimation of the parameters  $E_a$  and  $A$  using the Friedman method, a linear differential method that determines Arrhenius parameters without selecting a kinetic model [40]. The method is based on the following equation:

$$\ln \frac{d\alpha}{dt} = \ln A - \frac{E_a}{RT} + \ln f(\alpha) \tag{5}$$

where  $f(\alpha) = 1 - \alpha$  is a first-order reaction (Table 2).

### Results and discussion

Figure 1 shows the shrinkage curves obtained for samples N1–N4 in a dilatometer. As can be seen from the figure, the addition of zirconia affects sintering of multicomponent lithium ferrite.

During non-isothermal heating in the temperature range up to 600 °C, all the samples slightly expand. Then the length strongly changes due to a sharp densification of the samples at the non-isothermal sintering stage in the temperature range of 600–1010 °C. Here, the shrinkage rate in the process decreases when the concentration of zirconia additive grows. This leads to a decrease in the total shrinkage of the samples at the end of the non-isothermal sintering stage.

Figure 1 also shows that at the stage of isothermal heating further compaction of the samples occurs at a lower rate. However, at the end of sintering, the total shrinkage was almost similar for samples with low additive concentrations of up to 1 mass%. It should be noted that sample N4 with the addition of ZrO<sub>2</sub> 2 mass% shows the smallest degree of total compaction after sintering.

It is well known that ferrite sintering proceeds in several stages [41, 42]. At the initial sintering stage, when the

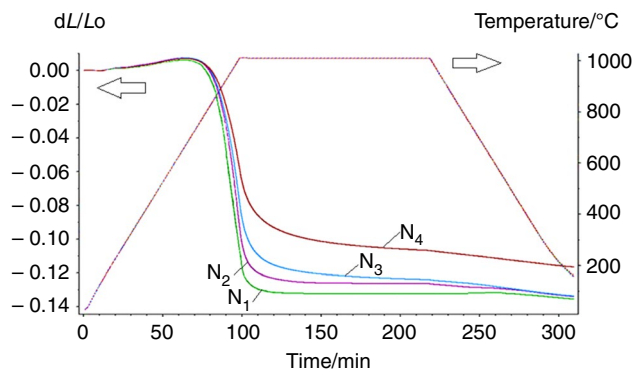


Fig. 1 Linear shrinkage and temperature regime of LiTiZn ferrite sintering in the dilatometer

porosity of the compact is high, samples are compacted due to particle sliding along the grain boundaries. The initial sintering stage involves the movement of grains, and it is completed upon achieving dense particle compaction. A distinctive feature of the initial sintering stage is significant shrinkage of the sample. Further, a decrease in porosity can occur due to mass transfer in the volume of particles, rather than transfer of particles as a whole. Apparently, the zirconia additive prevents an increase in the contact area between ferrite particles at the initial stage of sintering, reducing the compaction rate of ferrite samples.

At the next intermediate sintering stage, the sample is uniformly compacted. Its further shrinkage is accompanied by an increase in the contact area between the grains and approaching of their centers. At this stage, there are an intensive decrease in porosity and the isolation of pores from each other. In this case, the pores are located either at the grain boundaries or inside them. The further sintering stage is the slowest, therefore, long isothermal exposure is necessary to obtain a material with a high density. It is known that the process of sintering at these stages is determined by the mechanism of surface diffusion. As shown earlier in [29], the preliminary introduction of small amounts of zirconium dioxide before sintering leads to the preferential arrangement of its particles at the grain boundaries in sintered ferrites. It was also suggested that ZrO<sub>2</sub> can change the chemical composition of the samples due to the partial introduction of zirconium ions into the ferrite lattice. Therefore, this impurity possibly increases the concentration of vacancies near

Table 2 Mathematical models for kinetic analysis

Reaction type	Symbol	Function $f(\alpha)$
$n$ th-order reaction	$F_n$	$(1 - \alpha)^n$
Three-dimensional diffusion (Jander's type)	$D_3$	$1.5(1 - \alpha)^{1/3}((1 - \alpha)^{-1/3} - 1)$
Three-dimensional diffusion (Ginstling–Brounstein type)	$D_4$	$1.5/((1 - \alpha)^{-1/3} - 1)$

the surface of isolated pores, resulting in increased diffusion fluxes in this region and, thus, the overall shrinkage of the samples.

For samples N1–N4, the bulk density was calculated before and after sintering. Table 1 summarizes the data calculated for all samples. According to the data, the bulk density of the ferrites with  $ZrO_2$  ranging from 0 to 1 mass% increases. In contrast with this, the sample N4 exhibits the lowest density, which is consistent with dilatometric data.

In this study, only N2 samples were used to perform the kinetic analysis, since after sintering they are characterized by good bulk density (the relative density of ca. 96%) within the experimental error.

The results of the kinetic analysis performed by the Friedman method include graphs to show the dependence of the Arrhenius parameters on the conversion degree, in our case, on the shrinkage degree (Fig. 2a), and a graphical representation of the Friedman curve (Fig. 2b) represented by the function  $\log(d\alpha/dt) = f(1000 K T^{-1})$ . The Friedman analysis estimates kinetic parameters, but it does not provide a reaction kinetic model.

The dependences of the Arrhenius parameters on the conversion degree were estimated in the range of  $\alpha = 0–0.9$  (Fig. 2a). The graph shows that the parameters vary over the entire range of the conversion degree, which indicates a multi-stage pattern of sintering. The average values of these parameters can be used in the future to preliminarily estimate the Arrhenius parameters when modeling shrinkage curves using multivariate nonlinear regression. This approach allows estimation of the kinetic parameters of thermal sintering for multicomponent lithium ferrite using a physical process model.

The results of the Friedman analysis presented in Fig. 2b provide useful information about the nature of the processes occurring during ferrite sintering. The graph shows that the slope of the experimental curves (experimental points) is below the slope of the isoconversion lines (solid lines) at small conversion degrees. This indicates a diffusion reaction occurring during ferrite sintering. Therefore, the diffusion models shown in Table 2 were primarily considered in modeling through multivariate nonlinear regression.

The analysis showed that the experimental points of the compaction process obtained for sample N2 can be described

using a one-stage sintering mechanism. Table 3 presents the kinetic parameters obtained in modeling using the models considered in Table 2. The data provided in Table 3 show that an acceptable result, that is, a high value of the correlation coefficient, can be obtained using both the formal kinetic approach and the physical model of the process.

The best modeling results for the experimental curves and selected diffusion models were obtained using the Yander model with a correlation coefficient of 0.9997. Figure 3 shows the calculated curves to illustrate the modeling results. It should be noted that the Yander model can be used for diffusion processes. Moreover, it is suitable for describing the kinetics of the processes in powder systems with spherical particles [43]. However, simulation using the Ginstling–Brounstein model, which is a modified Yander model, led to similar kinetic parameters. One can notice that the activation energy values obtained from modeling via diffusion models are in good agreement with data presented in [44] for  $ZnFe_2O_4$  zinc ferrite, where the activation energy was in the range of 200–475  $\text{kJ mol}^{-1}$ .

At the same time, using the formal kinetic approach, the nature of the diffusion process can be estimated from the value of  $n$ . So, the  $n$  values equal to 0.33 and 0.5, correspond to the flow of diffusion along grain boundaries and bulk diffusion, respectively. In our work, modeling using an  $n$ -order equation led to  $n$  value of 0.39, which corresponds to the contributions of both diffusion processes during sintering of ferrite. In this case, the activation energy of the process is almost two times lower compared to the  $E_a$  obtained using the above diffusion models.

Structural defects and impurities play an important role in the sintering of ferrites, therefore in our case, the effect of

**Table 3** Kinetic parameters

Model	$\log A$	$E_a/\text{kJ mol}^{-1}$	$n$	Correlation coefficient
Diffusion models				
$D3$	$9.4 \pm 0.2$	$317.3 \pm 3.8$	–	0.9997
$D4$	$8.9 \pm 0.1$	$305.1 \pm 3.1$	–	0.9996
$n$ th-order reaction				
$F_n$	$2.2 \pm 0.1$	$132.7 \pm 3.4$	0.39	0.9991

**Fig. 2** Results of the Friedman analysis

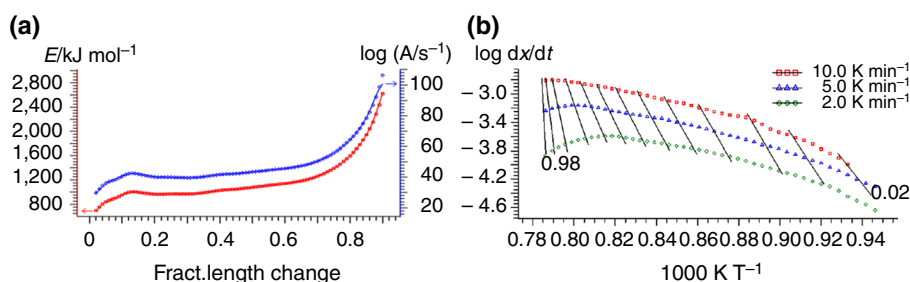
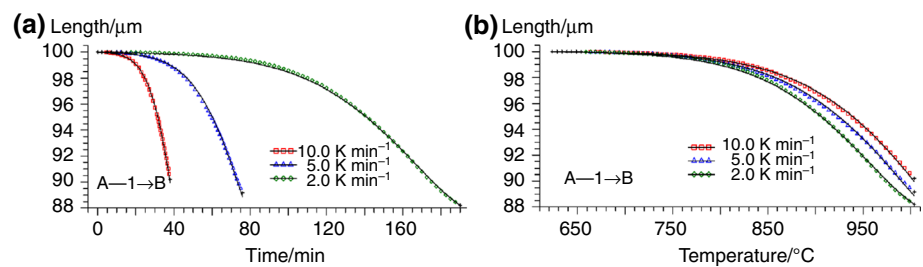


**Fig. 3** Modeling results of sintering in accordance with the 3-dim diffusion Jander's type reaction (symbols show experimental points, solid lines indicate calculated curves)



the ZrO<sub>2</sub> additive on sintering should be taken into account. The effect of the additive depends on its nature, concentration and distribution in the matrix. If the additive dissolves in the matrix, the concentration of point and linear defects and the diffusion mobility of the structural elements of the lattice change. As for the zirconia additive, it only partially dissolves in the matrix crystal [29], and its nanoparticles are uniformly distributed along the grain boundaries of lithium ferrite. Apparently, this impurity insignificantly prevents an intensive increase in the contact area between particles at the initial sintering stage, as shown by the shrinkage curves at the non-isothermal stage of samples heating. However, low concentrations of zirconia of up to 1 mass% have a significant effect on the final sintering stage, when the material porosity considerably decreases and isolated pores are healed.

Thus, comparison of the data obtained with the results of the previous study [29] shows that low concentrations of zirconia additives affect sintering of lithium ferrites and increase density of ferrite ceramics regardless of the ZrO<sub>2</sub> production method used. However, the percentage of this additive depends on the method employed to produce ZrO<sub>2</sub>. Therefore, up to 2 mass% of the plasma-chemical powder and up to 1 mass% of the powder prepared by sol-gel technique are required. Perhaps this is due to the prehistory of the ZrO<sub>2</sub> powder used, which consists in different phase composition and particle morphology. As known [34], the plasma-chemical powder is characterized by both a larger content of the monoclinic phase and a higher degree of agglomeration compared to the sol-gel powder. Additionally, the sol-gel powder was stabilized with yttrium oxide.

## Conclusions

The shrinkage behavior of compacts prepared from Li<sub>0.65</sub>Fe<sub>1.6</sub>Ti<sub>0.5</sub>Zn<sub>0.2</sub>Mn<sub>0.05</sub>O<sub>4</sub> multicomponent lithium ferrite with sol-gel ZrO<sub>2</sub> powder additive (0.5, 1 and 2 mass%) was investigated at different heating rates using dilatometric method.

A considerable difference in the shrinkage rate of ferrite compacts with different ZrO<sub>2</sub> content was observed in the non-isothermal heating stage of sintering. It was found that

the total ferrite compaction increases when the concentration of impurities grows up to 1 mass%. A further growth in ZrO<sub>2</sub> concentration decreases ferrite density.

Model-free Friedman and n-order reaction methods as well as diffusion models were used to determine the kinetic characteristics of shrinkage as a function of partial variation in their linear dimensions.

**Acknowledgements** The research was supported by RFBR Grant (Project No. 20-07-00662). The experiments on dilatometric analysis were funded from Tomsk Polytechnic University Competitiveness Enhancement Program.

## References

- Inoue A, Kong F. Soft magnetic materials. In: Reference module in materials science and materials engineering. Elsevier; 2020. <https://doi.org/10.1016/B978-0-12-803581-8.11725-4>.
- Mattei JL, Chevalier A, Laur V. Ferrite ceramics at microwave frequencies: applications and characterization. In: Reference module in materials science and materials engineering. Elsevier; 2020. <https://doi.org/10.1016/B978-0-12-803581-8.11765-5>.
- Teixeira SS, Amaral F, Graça MPF, Costa LC. Comparison of lithium ferrite powders prepared by sol-gel and solid state reaction methods. *Mater Sci Eng B*. 2020;255:114529.
- Darwish MA, Saafan SA, El-Kony D, Salahuddin NA. Preparation and investigation of dc conductivity and relative permeability of epoxy/Li-Ni-Zn ferrite composites. *J Magn Magn Mater*. 2015;385:99–106.
- Lysenko EN, Malyshev AV, Vlasov VA, Nikolaev EV, Surzhikov AP. Microstructure and thermal analysis of lithium ferrite pre-milled in a high-energy ball mill. *J Therm Anal Calorim*. 2018;134:127–33.
- Kotnala RK, Shah J, Singh B, Kishan H, Singh S, Dhawan SK, Sengupta A. Humidity response of Li-substituted magnesium ferrite. *Sens Actuat B*. 2008;129:909–14.
- Surzhikov AP, Pritulov AM, Lysenko EN, Sokolovskiy AN, Vlasov VA, Vasendina EA. Calorimetric investigation of radiation-thermal synthesised lithium penta-ferrite. *J Therm Anal Calorim*. 2010;101:11–3.
- Sharif M, Jacob J, Javed M, Manzoor A, Mahmood K, Khan MA. Impact of Co and Mn substitution on structural and dielectric properties of lithium soft ferrites. *Phys B*. 2019;567:45–50.
- Xu F, Shi X, Liao Y, Li J, Hu J. Investigation of grain growth and magnetic properties of low-sintered LiZnTi ferrite-ceramics. *Ceram Int*. 2020;46:14669–73.
- Xie F, Chen Y, Bai M, Wang P. Co-substituted LiZnTiBi ferrite with equivalent permeability and permittivity for high-frequency miniaturized antenna application. *Ceram Int*. 2019;45:17915–9.

11. Abu-Elsaad NI, Mazen SA, Salem HM. The effect of zinc substitution and heat treatment on microstructural and magnetic properties of Li ferrite nanoparticles. *J Alloys Compd.* 2020;835:155227.
12. Gao Y, Wang Z, Shi R, Pei J, Zhang H, Zhou X. Electromagnetic and microwave absorption properties of Ti doped Li–Zn ferrites. *J Alloys Compd.* 2019;805:934–41.
13. Lysenko EN, Surzhikov AP, Vlasov VA, Nikolaev EV, Malyshev AV, Bryazgin AA, Korobeynikov MV, Mikhailenko MA. Synthesis of substituted lithium ferrites under the pulsed and continuous electron beam heating. *Nucl Instr Methods Phys Res Sect B.* 2017;392:1–7.
14. Grusková A, Jančárik V, Sláma J, Dosoudil R. Effect of Zn–Ti substitution on electromagnetic properties of Li ferrites. *J Magn Mater.* 2006;304:e762–5.
15. Xu F, Shi X, Yang Y, Li J, Liao Y, Hu J. Enhanced magnetic properties of low temperature sintered LiZnTi ferrite ceramic synthesized through adjusting microstructure. *J Alloys Compd.* 2020;827:154338.
16. Xie F, Jia L, Xu F, Li J, Gan G, Zhang H. Improved sintering characteristics and gyromagnetic properties of low-temperature sintered  $\text{Li}_{42}\text{Zn}_{27}\text{Ti}_{11}\text{Mn}_1\text{Fe}_{21}\text{O}_4$  ferrite ceramics modified with  $\text{Bi}_2\text{O}_3\text{--ZnO--B}_2\text{O}_3$  glass additive. *Ceram Int.* 2018;44:13122–8.
17. Manonmani M, Jaikumar V, Gokul Raj S, Ramesh Kumar G. Crystallization, non-isothermal kinetics and structural analysis of nanocrystalline multiferroic bismuth ferrite ( $\text{BiFeO}_3$ ) synthesized by combustion method. *J Therm Anal Calorim.* 2019;138:185–93.
18. Dippong T, Cadar O, Levei E, Borodi G, Barbu-Tudoran L. Thermal behavior and effect of  $\text{SiO}_2$  and PVA- $\text{SiO}_2$  matrix on formation of Ni–Zn ferrite nanoparticles. *J Therm Anal Calorim.* 2019;138:3845–55.
19. Jalaiah K, Chandra Mouli K, Subba Rao PSV, Sreedhar B. Structural and dielectric properties of Zr and Cu co-substituted  $\text{Ni}_{0.5}\text{Zn}_{0.5}\text{Fe}_2\text{O}_4$ . *J Magn Mater.* 2017;432:418–24. <https://doi.org/10.1016/j.jmmm.2017.02.013>.
20. Almessiere MA, Slimani Y, Sertkol M, Nawaz M, Baykal A, Ercan I. The impact of Zr substituted Sr hexaferrite: investigation on structure, optic and magnetic properties. *Res Phys.* 2019;13:102244.
21. Jalaiah K, Vijaya Babu K, Chandra Mouli K, Subba Rao PSV. Effect on the structural, DC resistivity and magnetic properties of Zr and Cu co-substituted  $\text{Ni}_{0.5}\text{Zn}_{0.5}\text{Fe}_2\text{O}_4$  using sol–gel auto-combustion method. *Phys B Condens Matter.* 2018;534:125–33.
22. Kavitha S, Kurian M. Effect of zirconium doping in the microstructure, magnetic and dielectric properties of cobalt ferrite nanoparticles. *J Alloys Compd.* 2019;799:147–59.
23. El-Shater RE, El Shimy H, Assar ST. Investigation of physical properties of synthesized Zr doped Ni–Zn ferrites. *Mater Chem Phys.* 2020;247:122758.
24. Li LZ, Zhong XX, Wang R, Tu XQ. Structural, magnetic and electrical properties of Zr-substituted NiZnCo ferrite nanopowders. *J Magn Mater.* 2017;435:58–63.
25. Hua Z, Yao G, Ma J, Zhang M. Fabrication and mechanical properties of short  $\text{ZrO}_2$  fiber reinforced  $\text{NiFe}_2\text{O}_4$  matrix composites. *Ceram Int.* 2013;39:3699–708.
26. Sun B, Chen F, Xie D, Yang W, Shen H. A large domain wall pinning effect on the magnetic properties of  $\text{ZrO}_2$  added Mn–Zn ferrites. *Ceram Int.* 2014;40:6351–4.
27. Wang SF, Yang HC, Hsu YF, Hsieh CK. Effects of  $\text{SnO}_2$ ,  $\text{WO}_3$ , and  $\text{ZrO}_2$  addition on the magnetic and mechanical properties of NiCuZn ferrites. *J Magn Mater.* 2015;374:381–7.
28. Long X, Liu Y, Yao G, Du J, Zhang X, Cheng J, Hua Z. Microstructure and mechanical properties of  $\text{NiFe}_2\text{O}_4$  ceramics reinforced with  $\text{ZrO}_2$  particles with different sintering temperatures. *J Alloys Compd.* 2013;551:444–50.
29. Lysenko EN, Ghyngazov SA, Surzhikov AP, Nikolaeva SA, Vlasov VA. The influence of  $\text{ZrO}_2$  additive on sintering and microstructure of lithium and lithium-titanium-zinc ferrites. *Ceram Int.* 2019;45:2736–41.
30. Lysenko EN, Nikolaeva SA, Surzhikov AP, Ghyngazov SA, Plotnikova IV, Vlasov VA, Zhuravlev VA, Zhuravleva EV. Electrical and magnetic properties of  $\text{ZrO}_2$ -doped lithium-titanium-zinc ferrite ceramics. *Ceram Int.* 2019;45:20148–54.
31. Dippong T, Levei EA, Cadar O, Goga F, Borodi G, Barbu-Tudoran L. Thermal behavior of  $\text{Co}_x\text{Fe}_{3-x}\text{O}_4/\text{SiO}_2$  nanocomposites obtained by a modified sol–gel method. *J Therm Anal Calorim.* 2017;128:39–52.
32. Ștefănescu M, Dippong T, Stoia M, Ștefănescu O. Study on the obtaining of cobalt oxides by thermal decomposition of some complex combinations, undispersed and dispersed in  $\text{SiO}_2$  matrix. *J Therm Anal Calorim.* 2008;94:389–93.
33. Dippong T, Levei EA, Cadar O, Goga F, Toloman D, Borodi G. Thermal behavior of Ni, Co and Fe succinates embedded in silica matrix. *J Therm Anal Calorim.* 2019;136:1587–96.
34. Surzhikov AP, Ghyngazov SA, Frangulyan TS, Vasil'ev IP, Chernyavskii AV. Investigation of sintering behavior of  $\text{ZrO}_2$  (Y) ceramic green body by means of non-isothermal dilatometry and thermokinetic analysis. *J Therm Anal Calorim.* 2017;128:787–94.
35. Malyshev AV, Petrova AB, Surzhikov AP, Sokolovskiy AN. Effect of sintering regimes on the microstructure and magnetic properties of LiTiZn ferrite ceramics. *Ceram Int.* 2019;45:2719–24.
36. Opfermann J. Kinetic analysis using multivariate non-linear regression. *J Therm Anal Calorim.* 2000;60:641–58.
37. Ondro T, Húlan T, Al-Shantir O, Csáki Š, Václavů T, Trnák A. Kinetic analysis of the formation of high-temperature phases in an illite-based ceramic body using thermodilatometry. *J Therm Anal Calorim.* 2019;138:2289–94.
38. Brown ME, Dollimore D, Gallway AK. Reaction in solid state. *Comprehensive chemical kinetics.* Amsterdam: Elsevier; 1980.
39. Moukhina E. Determination of kinetic mechanisms for reactions measured with thermoanalytical instruments. *J Therm Anal Calorim.* 2012;109:1203–14.
40. Friedman HL. Kinetics of thermal degradation of char-forming plastics from thermogravimetry. Application to a phenolic plastic. *J Polym Sci Part C.* 1964;6:183–95.
41. Teo MLS, Kong LB, Li ZW, Lin GQ, Gan YB. Development of magneto-dielectric materials based on Li-ferrite ceramics I. Densification behavior and microstructure development. *J Alloys Compd.* 2008;459:557–66.
42. Thakur P, Chahar D, Taneja S, Bhalla N, Thakur A. A review on MnZn ferrites: synthesis, characterization and applications. *Ceram Int.* 2020;46:15740–63.
43. Wang Z, Liang Y, Peng N, Peng B. The non-isothermal kinetics of zinc ferrite reduction with carbon monoxide. *J Therm Anal Calorim.* 2019;136:2157–64.
44. Konvička T, Mošner P, Šolc Z. Investigation of the non-isothermal kinetic of the formation of  $\text{ZnFe}_2\text{O}_4$  and  $\text{ZnCr}_2\text{O}_4$ . *J Therm Anal Calorim.* 2000;60:629–40.

**Publisher's Note** Springer Nature remains neutral with regard to jurisdictional claims in published maps and institutional affiliations.